48th AIAA Aerospace Sciences Meeting Including the New Horizons Forum and Aerospace Exposition
4 - 7 January 2010, Orlando, Florida
AIAA 2010-965

Novel Multi-Barrier Plasma Actuators for Increased Thrust

Ryan Durscher* and Subrata Roy†
Computational Plasma Dynamics and Test Facility, Applied Physics Research Group
Mechanical and Aerospace Engineering Department
University of Florida, Gainesville, FL 32611-6300

This paper presents experimental measurements performed on multi-barrier plasma actuators (MBPA). The typical dielectric barrier discharge (DBD) plasma actuator consists of two electrodes separated by a dielectric layer. The surrounding air locally ionizes when a radio frequency (RF), high voltage waveform is applied to one of the electrodes. This results in an electrohydrodynamic (EHD) body force on the fluid. MBPAs extend upon the typical configuration of the DBD to incorporate multiple layers of dielectric materials and powered electrodes. This work explores different actuator designs which, through direct force balance measurements, demonstrate that the MBPA configuration effectively increases the EHD body force produced by a plasma actuator. The power consumption of these devices is analyzed and compared with typical actuator configurations. Results show significant increase in thrust over power ratio represented by actuator effectiveness.

Nomenclature

f	=	measured thrust, mN
I	=	instantaneous applied input current, A
l	=	length of electrode, mm
p	=	volume fraction of a dielectric layer
P_{tot}	=	total power delivered to the actuator, W
q	=	scaling exponent for power regression fitting
t	=	thickness of dielectric substrate, mm
V	=	instantaneous applied input voltage, kV
w	=	width of electrode, mm
β	=	relative phase angle
ε	=	relative dielectric constant
γ	=	effectiveness, mN/W
ϕ	=	peak applied potential, kV
ω	=	reference phase angle of driving potential

I. Introduction

Plasma actuation has been a topic which have received considerable attention in recent years within the fluid dynamics community. These devices have shown tremendous promise for various flow control applications. The dielectric barrier discharge (DBD), in particular, has successfully been shown both experimentally and numerically to control separation on airfoils, low pressure turbine blades and bluff bodies.[1-4] Unlike other flow control techniques such as mass injection, which may require a bulky mechanical system, the DBD is absent of moving parts. Additional advantages include near instantaneous response, relatively low power consumption and a wide range of operational frequencies. Unfortunately, to date, these benefits have not been fully utilized on a large scale since the effectiveness of these devices has been limited to low speed flows.

The DBD actuator is a rather simple device in design, with the typical configuration consisting of two thin electrodes placed asymmetrically on a dielectric material. The exposed electrode is powered with a radio frequency (RF) high voltage waveform, while the bottom electrode is grounded and usually encapsulated to prevent a discharge from occurring on the lower surface. Operational voltages and frequencies generally range from 5-20 kV_{pp}

* Graduate Student, Student Member AIAA, dursch@ufl.edu
† Associate Professor, Associate Fellow AIAA, roy@ufl.edu

and 1-20 kHz, respectively. Such a high potential difference weakly ionizes the surrounding gas in the vicinity of the exposed electrode, imparting an electrohydrodynamic (EHD) body force on the fluid. Aspects of these actuators such as the input waveform, geometric configuration, dielectric material, and driving frequency have been studied extensively in order to understand the relative importance of each parameter.[5-8] However, despite these efforts an optimized device capable of flow control at higher speeds has not been reached, for in general the maximum induced velocity, u_{max}, in a quiescent gas from a standard DBD actuator is typically 1~4 m/s. This in effect corresponds to a resultant thrust on the order of 0.1 g/m.[8,9]

In an effort to improve the thrust of DBD actuators, and to extend upon their usefulness we explore the concept of multi-barrier plasma actuators (MBPA)[10]. MBPAs are an extension upon the previously mentioned typical DBD actuator design which incorporate multiple layers of dielectric material and powered electrodes (Figure 1). This type of configuration adds additional parameters to the DBD actuator design space which need to be explored. In this paper we demonstrate that by controlling the relative phases of the input waveforms to the electrodes the potential difference can be increased and the plasma discharge extended. This results in an increase in the EHD body force. Experimental force balance measurements reveal that the MBPA design significantly improves the thrust production and power usage of a plasma actuator as compared to that of the standard design.

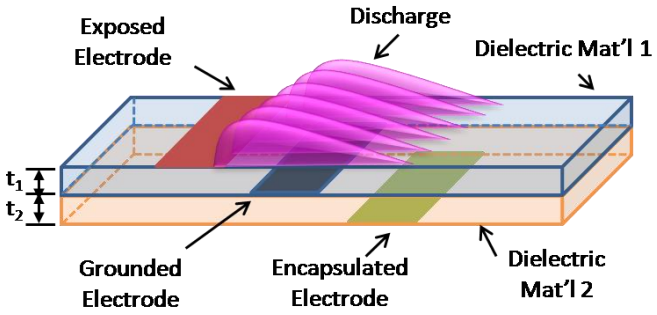

Figure 1. Multi-barrier plasma actuator schematic.[10]

II. Experimental Setup

A. Actuator Designs

Figure 2 shows a schematic representation of the actuators evaluated in this work. Cases 1, 2, and 3 correspond to various configurations of the standard actuator design with case 4 being the multi-barrier plasma actuator. Case 1 consists of an exposed electrode with a supplied potential, ϕ, driven at a reference phase angle, ω, of 0^o. In this design there are two asymmetrically placed grounded electrodes, one of which is sandwiched between the two dielectric layers. Case 2 has the same overall dimensions as case 1, although the middle grounded electrode has been removed. The voltage potential supplied to the exposed electrode has also been doubled for this case. For case 3, two actuators were constructed on a single layer of dielectric material. Both actuators are powered with the same potential and at the same relative phase. The arrangement is such as to take advantage of the peristaltic nature of the configuration. Case 4, the MBPA design, has the same geometric electrode layout as that of case 1. However, in this design the lower electrode is no longer grounded, but is instead supplied with a voltage potential that is -180^o out of phase relative to the exposed electrode (i.e. $\beta = -180^o$). Note that for all the cases with the exception of case 3 the distance between the edge of the exposed electrode and the right edge of the lowest or bottom electrode is the same (i.e. the same surface area). The reason for which case 3 is different will be outlined in the results discussion.

The dielectric material used to construct the actuators was acrylic which has a nominal dielectric constant, ε, of 3.0. The dielectric layer thicknesses, t_1 and t_2, were 2.0 and 1.5 mm, respectively, while the electrode width, w, was 2.0 mm. The acrylic layers were held together via a two part epoxy which for practical purposes is not assumed to play a role in the actuators operation. For all designs the electrodes had a length, l, of 130.0 mm and were constructed from 0.13 mm thick copper tape. A piece of standard electrical tape in combination with epoxy covered the bottom electrode to avert an unwanted discharge.

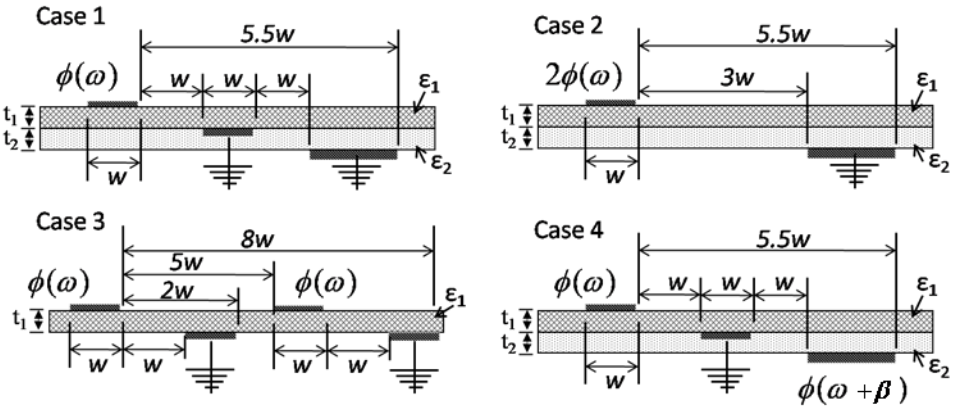

Figure 2. Schematic of actuator designs tested. Case 1-3 are considered to be variations on the standard actuator design, while the multi-barrier plasma actuator is represented by case 4. (Note: not to scale)

B. Plasma Generation and Power Measurements

In the present study, the powered electrodes were supplied with a high voltage, 14.0 kHz sinusoidal waveform. Since the MBPA design required two input signals, a dual output function generator (Tektronix AFG3022B) was used to generate the initial waveforms. The function generator allowed for precise control over the relative phase between the two driving signals. A dual output audio amplifier (QSC RMX2450) was used to further amplify the waveforms. The signals were split into two branches (1 and 2) and further increased using Corona Magnetics high-voltage, high-frequency power transformers. Figure 3 shows a schematic of the MBPA circuit. In the figure, branch 1 corresponds to the powering of the exposed electrode, while branch 2 denotes lower electrode. For the other cases (1-3) branch 2 was either grounded or not used.

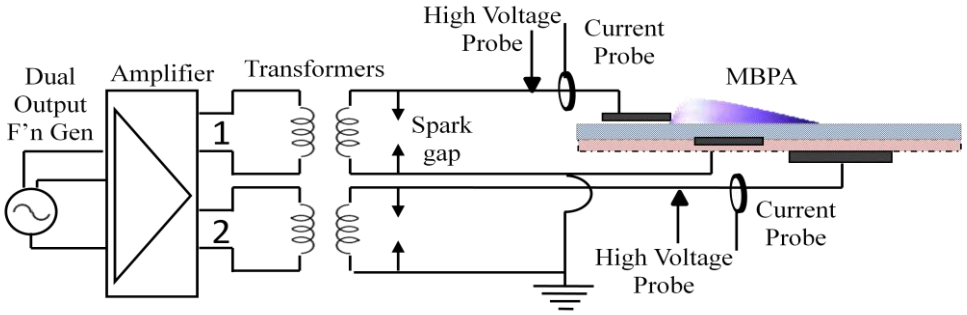

Figure 3. Plasma generation circuit used to power the multi-barrier plasma actuators.

High voltage probes (Tektronix P6015A) and ammeters (Pearson Electronics 2100) were used measure the voltage and current waveforms supplied to the actuators. These measurements were captured and monitored using a Tektronix DPO3054 oscilloscope. The current probes used in these experiments had a maximum bandwidth limit of 20.0 MHz. As such, to avoid erroneous measurements, it was necessary to implement a 20.0 MHz low-pass filter on the oscilloscope for said channels. In order to calculate the power delivered to the load, 1.0E6 samples were taken at a sampling rate of 250 MSamp/s. This corresponded to a total of 56 periods in a given data set. These measurements were then repeated five times at a given input voltage for an equivalent of 280 recorded periods. The total power, P_{tot}, delivered to the actuator was calculated by multiplying the instantaneous voltage, V_i, by the instantaneous current, I_i. The product was then summed and dived by the number of total measurements to give the average real power delivered (equation 1). The 1 and 2 subscripts found in equation 1 correspond to branches 1 and 2 of figure 3.

$$P_{tot} = \frac{1}{N}\left(\sum_{i=1}^{N} V_{i,1} I_{i,1} + \sum_{i=1}^{N} V_{i,2} I_{i,2}\right) \tag{1}$$

C. Force Measurements

The resultant thrust produced by the actuator was measured directly using an Ohaus (Adventurer™ Pro AV313C) precision balance. The resolution of the scale was ±1 mg. To negate electrostatic and/or electromagnetic interference, the scale was housed in an aluminum Faraday's cage with dimensions 30.5cm x 38.0 cm x 23.0 cm (width x depth x height). The actuator was then mounted on a stand which protruded approximately 20 cm from the top surface of the cage. This setup was contained within a larger quiescent chamber constructed of acrylic panels and an aluminum frame. The chambers dimensions were 0.61 m x 0.61 m x 1.22 m (width x depth x height). In order to minimize circuit losses heavily insulated high voltage wire was feed through the floor of chamber for the input leads. To prevent sagging wires from influencing the force measurements, thin magnetic wire (34AWG) was connected to the input leads. The overall setup used is similar to that of Hoskinson et al. and Opaits et al..[11,12] The balance was connected to a data acquisition computer which allowed the system to be control remotely through a user interface created in National Instruments LabVIEW software. The ability to view/record the displayed readout and re-zero the scale was built into the interface.

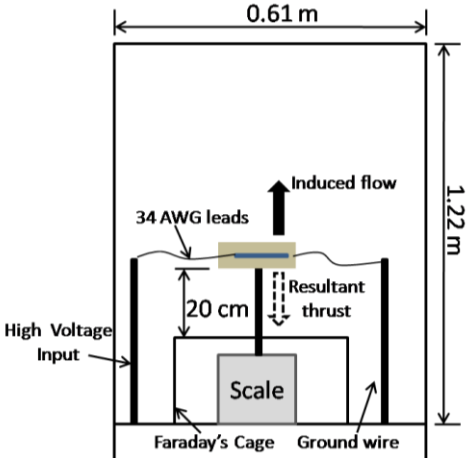

Figure 4. Experimental setup for direct force measurements. (Note: not to scale)

III. Results

A. Effective Electric Field

Since a variety of designs were tested, some using multiple layers of dielectric, it was necessary to formulate a common factor in order to make a fair comparison between each case. As a remedy, the use of equation 2 which has units corresponding to an electric field is proposed. As described previously ε and t denote the dielectric constants and thicknesses of the dielectric layers, respectively. The peak potential through each branch in the generation circuit is represented by ϕ.

$$\left(\varepsilon\phi/t\right)_{eff} = \left(\frac{\varepsilon_1\varepsilon_2}{t_1\varepsilon_2 + t_2\varepsilon_1}\right)\left(\phi_1 + \phi_2\right) \tag{2}$$

By considering a configuration similar to case 4, one can derive a generic formulation of equation 2 (figure 5a). In this actuator layout the supplied potential to the exposed electrode is at 90° phase shift with respect to a reference ground. Each subsequent electrode is at a point along the sinusoidal waveform such as its potential is less than that of the exposed electrode. The minimum potential is then reached at the bottom electrode, which is at a -90° phase relative to the exposed electrode. Furthermore, assuming the dielectric layers act as ideal capacitors, the path to the lowest potential then follows from the exposed electrode, through the middle electrodes, to finally the bottom electrode. From reference 13, an analogous circuit of the dielectric layers can then be drawn as a network of capacitors in series (figure 5b).[13] An equation for the effective dielectric constant can be written in terms of the volume fraction for the dielectric layer, *p*, divided by the dielectric constant for each layer, *i*, summed over n-layers.

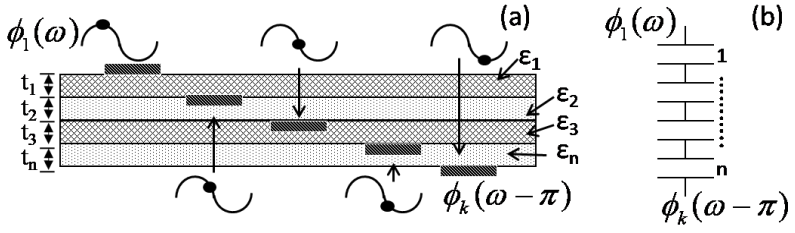

Figure 5. Schematic used in the generic derivation of an effective electric field: a) Actuator layout, b) Capacitor network in series.

$$\frac{1}{\varepsilon_{eff}} = \sum_{i=1}^{n} \frac{p_i}{\varepsilon_i} \tag{3}$$

For the cases tested the volume fraction simply becomes a ratio of the dielectric thickness to the total combined thicknesses. An example of the volume fraction for the first dielectric layer in case 4 is given by the following:

$$p_1 = \frac{t_1}{t_{tot}} = \frac{t_1}{t_1 + t_2} \tag{4}$$

Similarly, an effective electric field can be defined as the absolute value of the peak potential applied to each electrode divided by the total dielectric thickness as follows:

$$\left(\frac{\phi}{t}\right)_{eff} = \frac{1}{t_{tot}} \sum_{i=1}^{k-1} \left(\left|\phi_i\right| - \left|\phi_{i+1}\right| \right) \tag{5}$$

Solving now equation 3 for an effective dielectric constant and multiply by equation 5, one arrives at a generic form of equation 2 for n-layers of dielectric and k-electrodes. Although equation 2 pertains specifically to case 4, simplifications can be made by ignoring ϕ_2 and/or t_2 for cases 1, 2, and 3. This formulation takes into count the use of dielectric layers of various thicknesses as well as the use of different materials which could have varying dielectric constants. Although each dielectric layer used in these experiments had the same dielectric constant, this feature was included in the derivation in preparation for future efforts.

B. Force and Power Consumption Data

Force measurements were made over a range of input voltages. In the following results, 30 measurements were recorded at a sampling frequency of 0.5 Hz for each driving potential. Large variations in the measured force were observed if the measurements were made to soon after turning on the actuator. To prevent erroneous measurements the actuator was allowed to run for 3 minutes prior to taking data. Tests indicated that after a 3 minute warm up period a quasi-steady value was achieved. Due to the balance drifting, the actuator had to be turned off after the warm-up period and re-zeroed. The actuator was then immediately turned back on and sampling began. In between measurements the actuator was allowed to cool for 10 minutes before the process was repeated at a different input voltage.

The measured resultant force, *f*, divided by the exposed electrode length, *l*, for each case is presented in figure 6 over a range of effective input voltages. The data is fit with a linear interpolation which implies that there is a minimum voltage in which the plasma will ignite for each case. From the data it is clear that case 2 produces the greatest amount of thrust. However, while the MBPA design produces slightly less thrust than that of case 2, in comparison to cases 1 and 3 it does show a significant improvement in thrust production. Another observation which should be noted is that case 3 exhibits only slightly more thrust production than that of case 1, despite the fact that two actuators are being used as opposed to

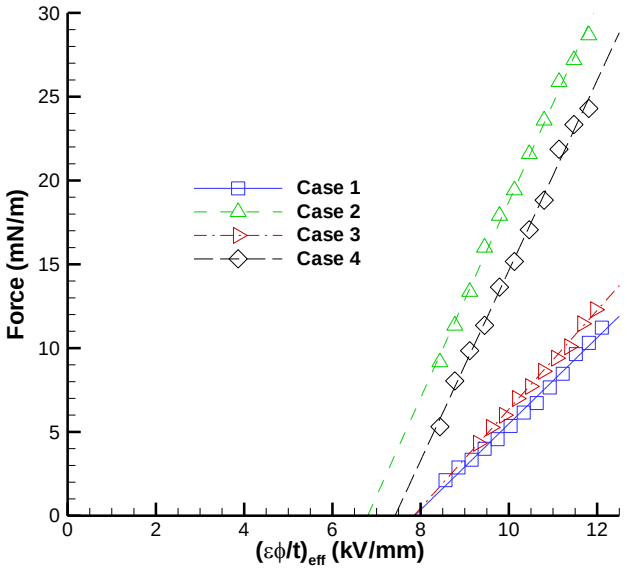

Figure 6. Force measurements over a range of effective electric fields for MBPA and standard actuator designs.

simply one. It was found for case 3 that if the pair of actuators were too close to each other, the powering of the consecutive (right) actuator would negatively affected the plasma formation on the first (left) actuator. Not only was a discharge in the opposite direction (than desired) observed, but the intensity of the plasma on the first actuator dwindled as the distance between the actuators decreased. As a result it was necessary to increase the separation between the actuators. As a guideline, the distance was increased to a point in which a discharge from the second actuator to the first actuator was no longer visually seen. This resulted in a spacing of 5*w* from what was originally intended to be 2.5*w*. Note that without this modification the surface area covered by the actuators would have remained the same for all the cases. However, referring to figure 5, this distance was clearly not optimal as the improvement in thrust production was only minimal.

Although case 2 was able to achieve higher values of thrust, its power consumption increased considerably compared to the other cases (figure 7). The power consumed in cases 3 and 4 were roughly the same since the same number of electrodes were powered in each design. Also note that while case 1 produced the least amount of force it also required the smallest amount of power. The data points presented in figure 6 are fit with a power regression of the form $y = ax^q$. The scaling exponent, q, for cases 1-4 are 3.28, 4.31, 3.38, and 3.86, respectively. These values correspond well to the 7/2 exponent power relation given in reference 7.

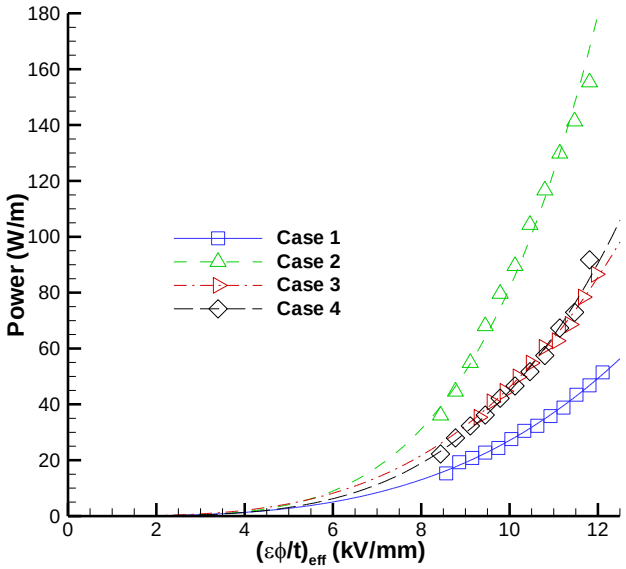

Figure 7. Power consumption over a range of effective electric fields for MBPA and standard actuator designs.

C. Effectiveness

As another means of comparing the actuator configurations, an effectiveness term, denoted as γ, is proposed. The effectiveness is defined as the ratio of the induced thrust to the consumed power (equation 6). This provides a better figure of merit, so to speak, than simply comparing which design can achieve more thrust. From system level design purposes, the configuration which can achieve higher thrust while consuming less power would be rightfully more desirable. Note that other authors have previously used this ratio to denote the efficiency of the actuator.[14] However, since the term efficiency is conventionally used to define a unitless parameter; it is not considered appropriate in this sense.

$$\gamma = f / P_{tot} \tag{6}$$

The effectiveness for each case is plotted in figure 7. Based on this analysis the multi-barrier plasma actuator significantly out performs all the other cases over the majority of potentials tested. This parameter emphasizes that although case 2 was able to achieve higher values of thrust; its power requirements were also much larger.

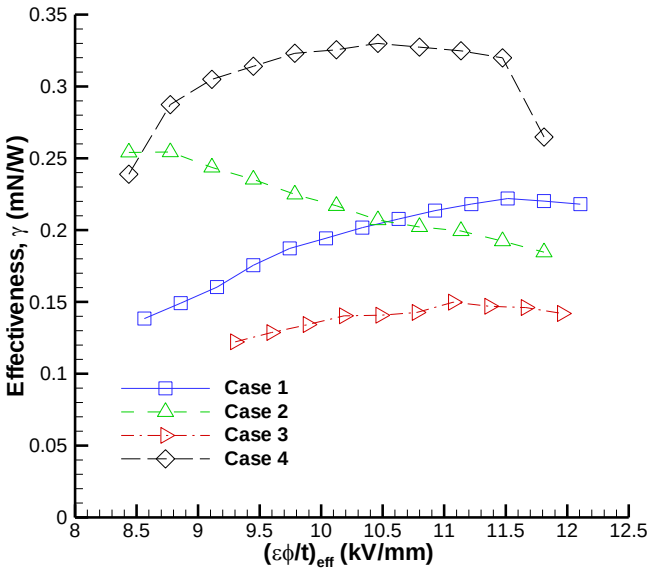

Figure 8. Thrust over power ratio represented by actuator effectiveness over a range of effective electric fields.

D. Phase Angle Dependency

To ensure that powering the lower electrode of the MBPA design (case 4) with a -180° phase shift was an optimal operation point, the influence of the relative phase angle on the resultant force was explored. Relative phase angles ranging from +180° to -180° were investigated. In the presented notation, positive values of β correspond to a leading phase angle, while negative values would be considered lagging. The measured force for both leading and lagging phase angles is plotted in figure 9. For phase angles between +100° and -100°, the discharge along the span of the actuator was no longer uniform. It was observed that for both the leading and lagging configuration, the discharge became noticeably weaker as the relative phase angles approached 0°. This resulted in a rapid decrease in thrust production.

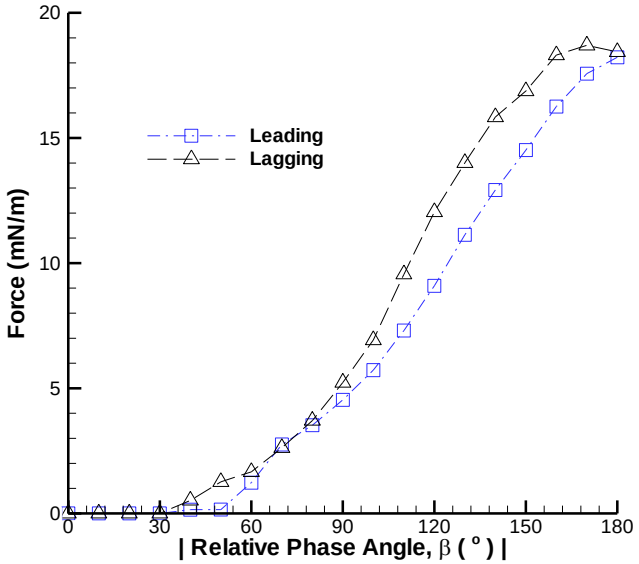

Figure 9. Effect of relative phase angle on the resultant force a MBPA configuration

Notably, even though the discharge eventually became sporadic, both the leading and lagging configurations follow the same general trend as the relative phase angle approaches 0°. However, from figure 9, a lagging circuit seems to be slightly more favorable in terms of maximum thrust production between angles -100° and -170°. In spite of this observation, when the force is plotted against power, both the lagging and leading data points collapse on top of each other (figure 10). This indicates that for a given amount of supplied power, the resultant force is indiscriminate to whether the relative phase angle is leading or lagging. A linear regression line is fitted though the datum (ignoring points in which the force was equal to 0) in figure 10. The linear fit reveals that the MBPA circuit consumes approximately 25 W/m regardless of a measurable force being present. Both the leading and lagging phase fits have slopes approximately equal to 0.5 mN/W.

Figure 10 demonstrates that the MBPA is nearly independent of a leading or lagging configuration on a force versus power basis. In close inspection, we see that slightly more power was consumed with a lagging circuit. We are investigating this phenomenon further.

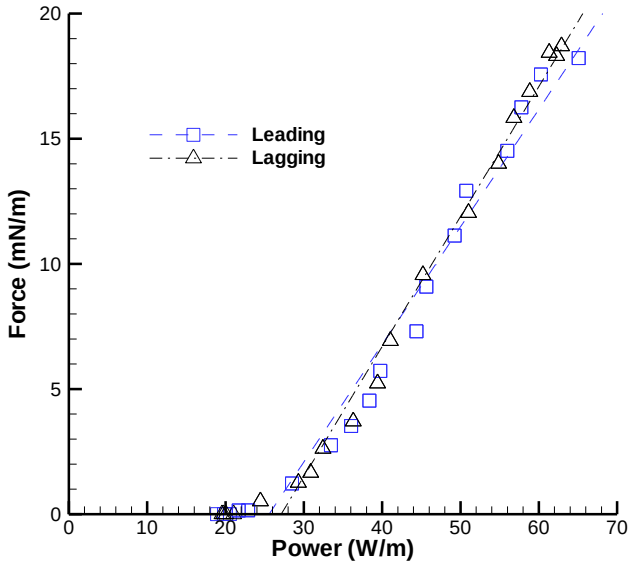

Figure 10. Induced force plotted against power consumption for leading and lagging relative phase angles.

IV. Conclusion

A novel multi-barrier plasma actuator design space is explored. The resultant thrust produced by DBD plasma actuators has been investigated for MBPA and various standard actuator configurations. It was found that the multi-barrier actuator was able to achieve a higher thrust production than two of the three standard designs evaluated. Based on the effectiveness, defined by the thrust over power ratio, the MBPA design significantly outperformed all of the standard actuator configurations. The effect of the relative phase angle of the supplied potential between the exposed and lower electrodes was also explored. It was found that the force was roughly independent of whether the potential of the lower electrode led or lagged the exposed electrode for a given consumed power. These initial results are quite encouraging. Experiments also indicate that at higher voltages, MBPAs are much more reliable than the standard actuators. Future plans entail further exploring this new design space in hopes of developing an optimized configuration. Aspects such as electrode configuration and relative phasing between electrodes need to be further investigated. Combining different dielectric materials of various thicknesses in n-layer configurations also requires evaluation.

Acknowledgements

This work was sponsored in part under Air Force Office of Scientific Research Grants #FA9550-09-1-0615 and #FA9550-09-1-0372 monitored by Drs. Doug Smith and Charles Suchomel.

References

[1]Huang, J., Corke, T. C., and Thomas, F. O., "Plasma Actuators for Separation Control of Low-Pressure Turbine Blades," *AIAA Journal*, Vol. 44, No. 1, 2006, pp 51- 57.

[2]Rizzetta, D. P. and Visbal, M.R, "Plasma-Based Flow-Control Strategies for Transitional Highly Loaded Low-Pressure Turbines," *J. Fluids Eng.*, Vol. 130, Issue 4, 2008.

[3]Visbal, M.R., Gaitonde, D. V., Roy, S., "Control of Transitional and Turbulent Flows Using Plasma-Based Actuators," *AIAA Fluid Dynamics Conference and Exhibit*, AIAA Paper 2006-3230, San Francisco, CA, June, 2006.

[4]Moreau, E., "Airflow control by non-thermal plasma actuators," *J. Phys. D: Applied Physics*, Vol. 40, 2007, pp.605-636.

[5]Abe, T., Takizawa, Y., Sato,S., and Kimura, N.,. "A Parametric Experimental Study for Momentum Transfer by Plasma Actuator." *45th AIAA Aerospace Sciences Meeting and Exhibit*, AIAA Paper 2007-187,Reno, NV, January, 2007.

[6]Roth, J. R., Dai, X., "Optimization of the Aerodynamic Plasma Actuator as an Electrohydrodynamic (EHD) Electrical Device," *44th AIAA Aerospace Sciences Meeting and Exhibit*, AIAA Paper 2006-1203, Reno, NV, January, 2006.

[7]Enloe, C. L., McLaughlin, T. E., VanDyken, R. D., Kachner, K. D., Jumper, E. J., Corke, T. C., Post, M., and Haddad, O., "Mechanisms and Responses of a Single Dielectric Barrier Plasma Actuator: Plasma Morphology," *AIAA Journal*, Vol. 42, No. 3, 2004, pp 589-594.

[8]Enloe, C. L., McLaughlin, T. E., VanDyken, R. D., Kachner, K. D., Jumper, E. J., Corke, T. C., Post, M., and Haddad, O., "Mechanisms and Responses of a Single Dielectric Barrier Plasma Actuator: Geometric Effects," *AIAA Journal*, Vol. 42, No. 3, 2004, pp 595- 604.

[9]Porter, C. O., Baughn, J. W., McLaughlin, T. E., Enloe, C. L., and Font, G. I., "Plasma Actuator Force Measurements," *AIAA Journal*, Vol. 45, No. 7, 2007, pp 1562- 1570.

[10]Roy, S., "Method and Apparatus for Multibarrier Plasma Actuated High Performance Flow Control," Patent WO 2009/005895, Published Jan 8, 2009 (filed May 2007).

[11]Hoskinson, A. R., Hershkowitz, N., Ashpis, D. E., "Force measurements of single and double barrier DBD plasma actuators in quiescent air," *J. Phys. D: Applied Physics.*, Vol. 41, 2008.

[12]Opaits, D. F., Zaidi, S. H., Shneider, M. N., Miles, R. B., Likhanskii, A. V., Macheret, S. O., and Ashpis, D., "Improving Thrust by Suppressing Charge Build-up in Pulsed DBD Plasma Actuators," *47th AIAA Aerospace Sciences Meeting Including The New Horizons Forum and Aerospace Exposition*, AIAA Paper 2009-487, Orlando, FL, January, 2009.

[13]Bergmsn, D., "The Dielectric Constant of a Composite Material – A Problem in Classical Physics," *Physics Report (Section C of Physics Letters)*, Vol. 43, No. 9, 1978, pp 377-403.

[14]Porter, C. O., Baughn, J. W., McLaughlin, T. E., Enloe, C. L., and Font, G. I., "Temporal Force Measurements on an Aerodynamic Plasma Actuator," *44th AIAA Aerospace Sciences Meeting and Exhibit*, AIAA Paper 2006-104, Reno, NV, January, 2006.